A model for predicting the relative chloride diffusion coefficient in unsaturated cementitious materials

Zhang, Yong; Ye, Guang

DOI
10.1016/j.cemconres.2018.10.013

Publication date
2019

Document Version
Accepted author manuscript

Published in
Cement and Concrete Research

A model for predicting the relative chloride diffusion coefficient in unsaturated cementitious materials

Yong Zhang[1*], Guang Ye[1]

[1] *Microlab, Section of Materials and Environment, Faculty of Civil Engineering and Geosciences, Delft University of Technology, Stevinweg 1, 2628 CN Delft, The Netherlands*

[*]Corresponding Author: Yong Zhang (y.zhang-1@tudelft.nl)

Abstract: An analytical model for predicting the *relative chloride diffusion coefficient* in cementitious materials at different degrees of water saturation is presented in this paper. The model is developed based on the Nernst-Einstein equation and conductivity of cementitious electrolyte, as well as on moisture distribution in the pore structure. Good agreement is found between the model and the experimental data. With the help of the model, the chloride diffusion coefficient of cementitious material at *unsaturated* state can be determined according to the chloride diffusion coefficient at *saturated* state, the degree of water saturation and the average pore diameter of the material. A detailed discussion about the inputs and outputs of the model is given in order to facilitate its application for engineering practice.

Keywords: Modeling; Chloride diffusion; Degree of water saturation; Pore structure; Cementitious material

1. Introduction

1.1. Research background

Durability problems associated with chloride-induced corrosion of reinforcement in concrete structures have drawn considerable attention over the past decades. Reliable prediction of the chloride penetration in concrete cover is of high interest. In most service life design and durability specifications, e.g. DuraCrete [1] and Life-365 [2], the chloride penetration is assumed to be governed by diffusion of chloride ions in the pore structure of concrete [3]. The chloride diffusion coefficient is a parameter widely used to indicate the capacity of concrete to resist chloride diffusion.

Chloride diffusion in concrete is a moisture-dependent process. Onsite concrete is often *partially saturated* with water [4-6]. Even for a concrete after two years' immersion in sea water, the moisture conditions of internal concrete (deeper than 20-30 mm) still depend on the early self-desiccation, e.g. with a degree of water saturation of around 85% [7]. The moisture content, and the manner in which the moisture distributes in the pore structure, can have profound impacts on the chloride diffusion coefficient [8].

In present service life calculations, e.g. DuraCrete [1], the chloride diffusion coefficient is generally determined based on chloride penetration tests performed on *saturated* concretes. The effect of the moisture condition on the chloride diffusion is implicitly described with the ageing factor n and the environment factor k_e. In the absence of long term exposure data, the determination of the ageing factor n and the environment factor k_e largely depends on experts and their opinions. This may introduce risks or uncertainties in new structure design. To achieve accurate service life prediction, the development of reliable model(s) to determine

the chloride diffusion coefficient in *unsaturated* concretes is essential. Such model(s) will help the designer to better understand the actual serviceability of concrete structures.

1.2. Literature survey

The *relative chloride diffusion coefficient* D_{rc} has often been used to describe the chloride diffusion in partially saturated cementitious materials [8]. It is defined as a ratio of chloride diffusion coefficient at a particular unsaturated state over that at saturated state. The unsaturated state, in the case where equilibrium moisture content is present, can be indicated by either the degree of water saturation S_w or the internal relative humidity RH.

A few experimental works have contributed to clarifying the dependency of the ionic diffusion on moisture content. Attempt to model the relative chloride diffusion coefficient D_{rc} of concrete dates back to the late 20th century. Maybe Saetta et al. [9] were the first who proposed an *S-shaped* relationship (Eq. (1)) to describe the D_{rc} as a function of decreasing RH in concrete.

$$D_{\mathrm{rc}} = \frac{D(\mathrm{RH})}{D(\mathrm{RH} = 100\%)} = \left[1 + \frac{(1 - \mathrm{RH})^4}{(1 - \mathrm{RH_c})^4}\right]^{-1} \quad (1)$$

A predefined *critical relative humidity* RH_c, at which D_{rc} = 0.5, has to be adopted for applying the S-shaped relationship. RH_c = 75% was given in the work of Saetta et al. [9]. A different RH_c-value of 88% was reported by Nielsen and Geiker [10] who applied Eq. (1) to describe the chloride diffusion coefficients of unsaturated mortars. Other recent reports on the subject of non-saturated ionic transport [8, 11, 12] also indicated that the RH_c-value is not a constant but may vary in a wide range of 75~92%, depending on the temperature and the pore structure of the samples used. The fact that adoption of different RH_c-values can result in

significantly different D_{rc}-RH relationships is a great obstacle to effectively apply the S-shaped relationship in engineering practice.

Buchwald [13] estimated the ionic diffusion coefficient in masonry materials based on impedance spectroscopy measurements. A semi-empirical *power* equation shown in Eq. (2), which relates the D_{rc} to the degree of water saturation S_w, was put forward.

$$D_{rc} = \frac{D(S_w)}{D(S_w = 1)} = {S_w}^{\lambda} \tag{2}$$

where λ is a fitting parameter. A few researchers have used the power equation (Eq. (2)) to fit the experimental data produced in their works. Baroghel-Bouny et al. [14] found $\lambda = 6$ and Olsson et al. [12] found $\lambda = 4.5$. The origin of the power equation (Eq. (2)) can be traced to the well-known Archie's second law [15], which empirically relates the electrical conductivity to the porosity and degree of water saturation S_w. However, the power equation (Eq. (2)) cannot fully account for the dependency of ionic diffusion on the water saturation level, since the aspects with respect to how and where the pore space is water-filled, especially to what extent the water-filled pores are connected allowing ionic transport, are not considered.

Based on simulated microstructures, Zhang et al. [16] studied the ionic diffusion in unsaturated cement pastes with water-to-cement (w/c) ratios of 0.4, 0.5 and 0.6 by using lattice Boltzmann method. He suggested a quadratic *polynomial* equation, as shown in Eq. (3), with which the simulated D_{rc}-S_w relations could be approximately described.

$$D_{rc} = \frac{D(S_w)}{D(S_w = 1)} = a \cdot {S_w}^2 + b \cdot S_w + c \tag{3}$$

where a, b and c are empirical constants.

It should be emphasized that the experimental data reported in literature cannot be well described with the existing equations. Figure 1a shows an example of the curves obtained by using Eqs. (2) and (3) to fit the data taken from Rajabipour [17]. It is shown that the power equation (Eq. (2)) tends to underestimate the D_{rc}-value at high saturation levels (e.g. S_w > 85%) and overestimate the D_{rc}-value at low saturation levels (e.g. S_w < 85%). The polynomial equation (Eq. (3)) is capable to describe the D_{rc}-S_w plots only for $S_w \geq 64\%$, but becomes ineffective when S_w < 64%. Figure 1b compares the S-shaped relationship (Eq. (1)) with the experimental data (D_{rc} *vs.* RH) taken from two different reports [10, 12]. It can be concluded that the S-shaped relationship overestimates the D_{rc}-value at high RH levels (e.g. RH > 85%) and underestimates the D_{rc}-value at low RH levels (e.g. RH < 85%).

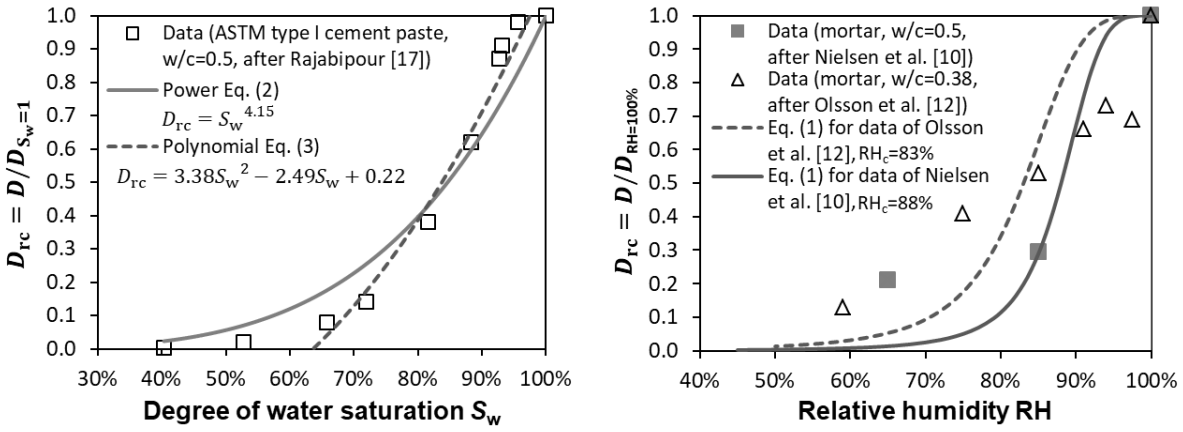

(a) (b)

Fig. 1. Comparison between existing equations (Eqs. (1), (2) and (3)) and experimental data about relative chloride diffusion coefficient D_{rc}: (a) D_{rc} *vs.* S_w; (b) D_{rc} *vs.* RH

The D_{rc}-S_w (or D_{rc}-RH) data published in the literature exhibit a large scatter [8]. The existing equations (Eqs. (1), (2) and (3)), obtained based on curve fittings, should be judged as phenomenological calculation procedures. There is not a broad agreement between these equations and experimental data published. Further study has to be done in order to establish a more reliable D_{rc}-S_w (or D_{rc}-RH) model for engineering practice.

1.3. Scope and aim of the present work

The challenges of establishing reliable D_{rc}-S_w (or D_{rc}-RH) models can be ascribed primarily to the intrinsic complexity of the pore structure of cementitious materials. There are three different pore categories: *connected pores* that can form a connected network relating the two opposite surfaces of a porous specimen, *dead-end pores* that are connected with only one surface of a porous specimen, and *isolated pores* that have no connection with any surface of a porous specimen.

The differences with respect to the ionic transport between saturated and unsaturated pore systems are illustrated in Fig. 2. In saturated pore system (Fig. 2a), the dead-end and isolated pores do not contribute to ionic transport while the rest pores (i.e. connected pores) are all able to provide paths for ionic transport. In unsaturated pore system (Fig. 2b), the water phase accumulates preferentially in the small pores and the large pores tend to be filled with the gas phase. The connected pores can then be categorized into three groups: (i) *Gas-filled pores*, which impede the ionic transport; (ii) *Discontinuous water-filled pores*, which refer to the pores that are water-filled but cannot form a continuous path for ionic transport; (iii) *Continuous water-filled pores*, which are able to form an interconnected water-filled network for ionic transport. For a given degree of water saturation S_w, the continuity of water-filled pores determines the rate of ionic transport in unsaturated pore systems.

The continuity of water-filled pores depends not only on the moisture content but also on the moisture distribution in the pore structure. All parameters that affect the pore structure will inevitably alter the moisture distribution and hence the D_{rc}-S_w relations. The emphasis of current equations (Eqs. (1), (2) and (3)) is mainly on *moisture content*. The *pore structure* is a fundamental factor influencing the moisture distribution and has to be further considered in order to reliably predict the D_{rc}-value.

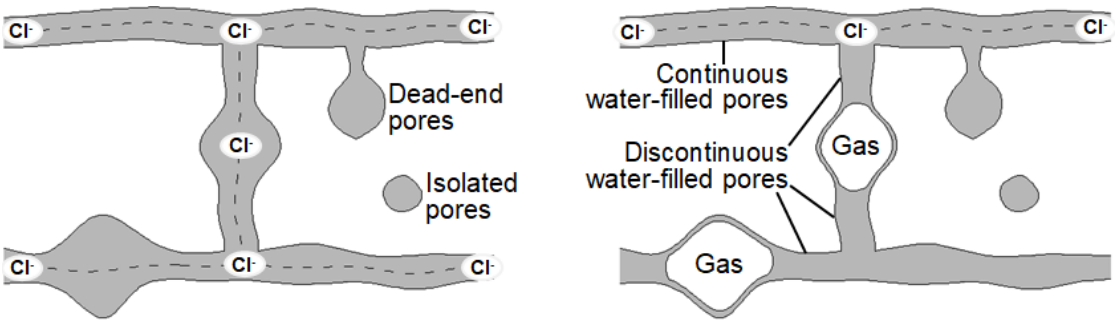

(a) Saturated (b) Unsaturated

Fig. 2. Schematic representations of the moisture distribution and chloride (Cl^-) transport in pore systems

The aim of the present work is to develop a model, with which the relative chloride diffusion coefficient D_{rc} can be predicted based on the degree of water saturation S_w and the pore structure of cementitious material. The work is organized in three parts.

1) Model development: On the basis of the Nernst-Einstein equation [18], the chloride diffusion coefficient of cementitious material is determined from its conductivity. The conductivity of cementitious material is linked to the microstructural parameters. The moisture distribution at different degrees of water saturation S_w is estimated from water vapour desorption isotherm. An analytical model for describing the D_{rc}-S_w relationship is then established.

2) Validation of the model: Resistivity measurements are carried out on mortar specimens preconditioned at different degrees of water saturation S_w. The pore structure of paste specimens is measured by the mercury intrusion porosimetry technique. The D_{rc}-S_w relations obtained from the experiments are used to validate the model established above. Validation of the model with the experimental data reported in the literature is performed as well.
3) Discussion: A few aspects related to the applicability of the model for engineering practice are discussed.

2. Modeling of relative chloride diffusion coefficient

The chloride diffusion in cementitious materials is influenced by a variety of physical and chemical factors, such as water content, pore structure, chloride binding, ion-ion interaction, ion-pore wall interaction etc. More details about the chloride diffusion mechanisms in cementitious materials can be referred to Refs. [19, 20]. It is far from easy to model the relative chloride diffusion coefficient covering all the influencing factors. The present work is specifically dedicated to model the effects of *water content* and *pore structure* on chloride diffusion.

Modeling of the relative chloride diffusion coefficient will be performed based on the Nernst-Einstein equation and conductivity of cementitious electrolyte, as well as on moisture distribution in the pore structure. Three assumptions are made in the modeling: (i) chloride binding and electrochemical effects on chloride diffusion are not taken into account; (ii) cementitious material at any particular degree of water saturation exhibits a homogeneous moisture distribution, i.e. the relative humidity is uniform in the material; (iii) all pore water is regarded as a solute.

2.1. Nernst-Einstein equation

If cementitious material is considered to be a solid electrolyte, the diffusion of charged species in cementitious material can be related to its partial conductivity. The relation is described by the Nernst-Einstein equation [18]. As shown in Eq. (4), the ratio of conductivity σ_{p} of the pore solution to conductivity σ [S/m] of the cementitious material is equal to the ratio of chloride diffusion coefficient D_{p} in the pore solution to chloride diffusion coefficient D [$\mathrm{m^2/s}$] in the cementitious material. In geoscience literature this ratio is defined as formation factor F_0 [21].

$$F_0 = \frac{\sigma_{\mathrm{p}}}{\sigma} = \frac{D_{\mathrm{p}}}{D} \tag{4}$$

The D_{p}-value is around 1.5×10^{-9} $\mathrm{m^2/s}$ at room temperature when the chloride concentration is in the range of 0.1~1.0 mol/L [22]. For an unsaturated cementitious material the D-value can be calculated from the σ-value, after correcting the σ_{p}-value for the water saturation level.

2.2. Conductivity σ of cementitious material

2.2.1. Conductivity σ as a function of the degree of water saturation

The conductivity σ of cementitious material is the inverse of its resistivity ρ [Ω·m], as shown in Eq. (5) [23].

$$\sigma = \frac{1}{\rho} = \frac{mL}{A} \cdot \frac{1}{R} \tag{5}$$

where m is the geometry factor (m = 1 for cylindrical specimen); L [m], A [$\mathrm{m^2}$] and R [Ω] represent the length, the cross sectional area and the electrical resistance, respectively. For

183 direct current the electrical resistance *R* is determined by Ohm's law and equal to the ratio of
184 the voltage applied to a specimen's ends over the current passing through.

185 In cementitious materials the conductivity of the pore solution phase, σ_{p}, is usually many
186 orders of magnitude higher than that of the solid phase, σ_{s}, and the vapour phase, σ_{v}. As
187 reported in Refs. [24, 25], σ_{p} is in the range of 1~20 S/m, σ_{s} is around 10^{-9} S/m and σ_{v} is in
188 the order of 10^{-15} S/m. Hence the conductivity σ of cementitious material can simply be
189 described by Eq. (6).

$$\sigma = \sigma_{\mathrm{p}} \phi_{\mathrm{p}} \beta_{\mathrm{p}} \tag{6}$$

190 where ϕ_{p} is the volume fraction of the pore solution phase; β_{p} is a structure factor accounting
191 for the effect of the actual structure of the pore solution phase on ionic conduction. The
192 structure factor β_{p} of the pore solution phase is related to the interconnected water-filled
193 pores, which depend on the pore structure characteristics (indicated by a parameter μ_{p}
194 accounting for pore connectivity and tortuosity [26]) and the moisture distribution (indicated
195 by the continuity η_{w} of water-filled pores). Quantitative description of the continuity η_{w} of
196 water-filled pores is presented in the next section.

197 At *saturated* state (S_{w} = 100%), the volume fraction ϕ_{p} of the pore solution phase is equal to
198 the total porosity ϕ_{t} of the cementitious material. The structure factor β_{p} of the pore solution
199 phase is determined by the pore structure parameter μ_{p} alone. Equation (6) is rewritten as Eq.
200 (7).

$$\sigma_{\mathrm{Sat}} = \sigma_{\mathrm{p,Sat}} \cdot \phi_{\mathrm{t}} \cdot \mu_{\mathrm{p}} \tag{7}$$

where σ_{Sat} is the conductivity of the cementitious material at saturated state; $\sigma_{\mathrm{p,Sat}}$ is the conductivity of the pore solution at saturated state.

At *unsaturated* state (S_{w} < 100%), the volume fraction ϕ_{p} of the pore solution phase is equal to $\phi_{\mathrm{t}}S_{\mathrm{w}}$. The structure factor β_{p} of the pore solution phase is determined by both the pore structure parameter μ_{p} and the continuity η_{w} of water-filled pores, as $\beta_{\mathrm{p}} = \mu_{\mathrm{p}}\eta_{\mathrm{w}}$. Equation (7) is then modified as Eq. (8).

$$\sigma_{\mathrm{S_w}} = \sigma_{\mathrm{p,S_w}} \cdot \phi_{\mathrm{t}}S_{\mathrm{w}} \cdot \mu_{\mathrm{p}}\eta_{\mathrm{w}} \tag{8}$$

where $\sigma_{\mathrm{S_w}}$ is the conductivity of the cementitious material at a particular water saturation level; $\sigma_{\mathrm{p,S_w}}$ is the conductivity of the pore solution at a particular water saturation level.

2.2.2. Water continuity η_w as a function of the degree of water saturation

The continuity of water-filled pores, in short water continuity η_{w}, stands for the effect of the moisture distribution on the ionic transport in a porous system. The water continuity η_{w} is related to the extent of the interconnection of water-filled pores. Ionic transport occurs only if a continuous water-filled path is present.

The water continuity η_{w} as a function of the degree of water saturation S_{w} can be estimated from the sorption isotherm of the pore system. The sorption isotherm illustrates the changes of the relative humidity RH with different saturation levels S_{w}. According to Kelvin's law [27], RH corresponds to the diameter d_{m} of the meniscus. Considering the thickness t of the adsorbed water film, the pores below the diameter d_{p} ($d_{\mathrm{p}} = d_{\mathrm{m}} + 2t$) are fully water-filled. Combining the RH-S_{w} relation with the RH-d_{p} relation enables to determine the d_{p}-S_{w} relation.

The d_p-S_w relation is used to describe the distribution of water-filled pores in an unsaturated pore system. It is considered that water loss in the dead-end and isolated pores will not influence the internal RH of the pore system, and hence does not alter the smallest drained pore diameter d_p. This, in turn, reveals that a decrease of the d_p-value should result from the occurrence of water loss in the connected pores and will reduce the continuous water-filled paths, leading to a lower water continuity η_w.

An example of the d_p-S_w relations, obtained from water vapour desorption isotherm tests previously presented in Ref. [28], is shown in Fig. 3. The d_p-value changes substantially in the high saturation levels (i.e. $60\% \leq S_w \leq 100\%$) while changes slightly in the low saturation levels (i.e. $S_w < 60\%$). The d_p-S_w plots can be approximated with a power equation shown in Eq. (9). The correlation coefficients are 0.96, 0.95 and 0.93 for specimens with w/c ratios of 0.4, 0.5 and 0.6, respectively.

$$d_p = \frac{2c^2}{(1-S_w)^2} \cdot d_0 \tag{9}$$

where d_0 is the diameter for one-unit length pore (herein, d_0 = 1 nm); $2c^2/(1-S_w)^2$ is a moisture distribution factor, in which the coefficient c is related to the distribution of water-filled pores and depends primarily on the pore size distribution of the specimen. A smaller c value corresponds to a specimen with a lower w/c ratio (i.e. a finer pore size distribution).

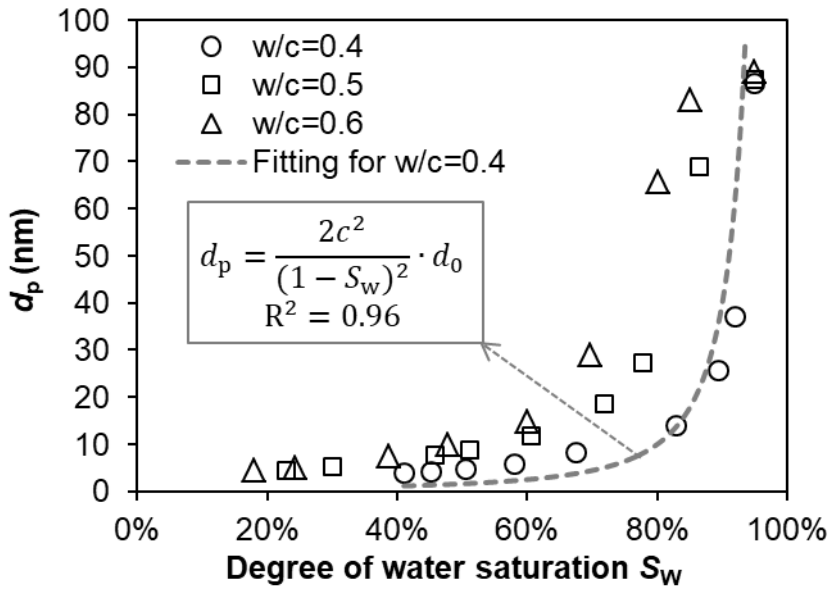

236

237 **Fig. 3.** Moisture distribution (d_p-S_w) estimated from water vapour desorption isotherm tests of
238 one-year-old cement mortars (w/c = 0.4, 0.5 and 0.6). The data are taken from Ref. [28]. d_p is
239 the smallest drained pore diameter determined by the Kelvin-Cohen equation [29]

240

241 The water continuity η_w is controlled mainly by the water-filled pores (with diameter $d \leq d_p$).
242 Both d_p-value and η_w-value depend on the degree of water saturation S_w. In a saturated pore
243 system (S_w = 100%), $d_p \rightarrow \infty$ and $\eta_w = 1$. When the pore system is drained (S_w approaching
244 zero), $d_p \rightarrow 0$ and $\eta_w \rightarrow 0$. The η_w-d_p relationship that satisfies the two boundary conditions
245 can be described with an exponential equation shown in Eq. (10).

$$\eta_w = e^{-\frac{d_0}{d_p}} \tag{10}$$

246 Combining Eq. (9) and Eq. (10) leads to an expression for the water continuity of unsaturated
247 cementitious materials.

$$\eta_{\mathrm{w}} = e^{-\frac{(1-S_{\mathrm{w}})^2}{2c^2}} \tag{11}$$

Equation (11) can be used to predict the water continuity η_{w} at various degrees of water saturation S_{w}, provided that the coefficient c of the material of interest is known. Equation (11) is a form of Gaussian function. The fact that the pore size distribution of cementitious materials (estimated by MIP tests) also shows a Gaussian distribution [30] confirms the pronounced dependency of the water continuity on the pore size distribution.

2.3. Relative chloride diffusion coefficient D_{rc}

The relative chloride diffusion coefficient D_{rc} is expressed as the ratio of chloride diffusion coefficient $D_{\mathrm{S_w}}$ at a particular degree of water saturation over chloride diffusion coefficient D_{Sat} at saturated state. Based on the Nernst-Einstein equation (Eq. (4)), the $D_{\mathrm{S_w}}$ and the D_{Sat} can be calculated with Eq. (12a) and Eq. (12b), respectively.

$$D_{\mathrm{S_w}} = \frac{\sigma_{\mathrm{S_w}}}{\sigma_{\mathrm{p,S_w}}} \cdot D_{\mathrm{p}} \tag{12a}$$

$$D_{\mathrm{Sat}} = \frac{\sigma_{\mathrm{Sat}}}{\sigma_{\mathrm{p,Sat}}} \cdot D_{\mathrm{p}} \tag{12b}$$

Combining Eq. (12a) with Eq. (12b) leads to the expression for the relative chloride diffusion coefficient.

$$D_{\mathrm{rc}} = \frac{D_{\mathrm{S_w}}}{D_{\mathrm{Sat}}} = \frac{\sigma_{\mathrm{S_w}}}{\sigma_{\mathrm{Sat}}} \cdot \frac{\sigma_{\mathrm{p,Sat}}}{\sigma_{\mathrm{p,S_w}}} \tag{13}$$

Substituting Eqs. (7) and (8) into Eq. (13) gives:

$$D_{\mathrm{rc}} = \frac{D_{\mathrm{S_w}}}{D_{\mathrm{Sat}}} = S_{\mathrm{w}} \cdot \eta_{\mathrm{w}} \tag{14}$$

Substituting Eq. (11) into Eq. (14) allows the D_{rc} to be computed straightforwardly from the analytical model expressed in Eq. (15).

$$D_{\mathrm{rc}} = \frac{D_{\mathrm{S_w}}}{D_{\mathrm{Sat}}} = S_{\mathrm{w}} \cdot e^{-\frac{(1-S_{\mathrm{w}})^2}{2 \cdot c^2}} \tag{15}$$

where the coefficient c is larger in a cementitious material with coarser pore size distribution. As will be shown in Section 5.3, the coefficient c is a function of the average pore diameter and the c-value is usually in the range 0~0.45 for hydrated cementitious materials.

Figure 4 shows the D_{rc}-S_{w} curves calculated by Eq. (15) with the coefficient c varying from 0.05 to 0.9. At c = 0.05, the D_{rc}-value is highly dependent on the degree of water saturation S_{w}. Such dependency, however, becomes less pronounced in a cementitious material with higher c-value. The D_{rc}-S_{w} relationship is almost linear for $c \geq 0.7$.

In Eq. (13) the parameters σ_{Sat}, $\sigma_{\mathrm{S_w}}$, $\sigma_{\mathrm{p,Sat}}$ and $\sigma_{\mathrm{p,S_w}}$ are obtainable from conductivity experiments. The values of $\sigma_{\mathrm{S_w}}$ and σ_{Sat} can be determined from resistivity measurements on cementitious materials. The values of $\sigma_{\mathrm{p,S_w}}$ and $\sigma_{\mathrm{p,Sat}}$ rely on the pore solution chemistry that differs with changing degree of water saturation S_{w}. The experimental D_{rc}-S_{w} data (Eq. (13)) will be used to validate the mathematical D_{rc}-S_{w} relation (Eq. (15)). Meanwhile the coefficient c in Eq. (15) will be determined. The experimental details are presented in the following.

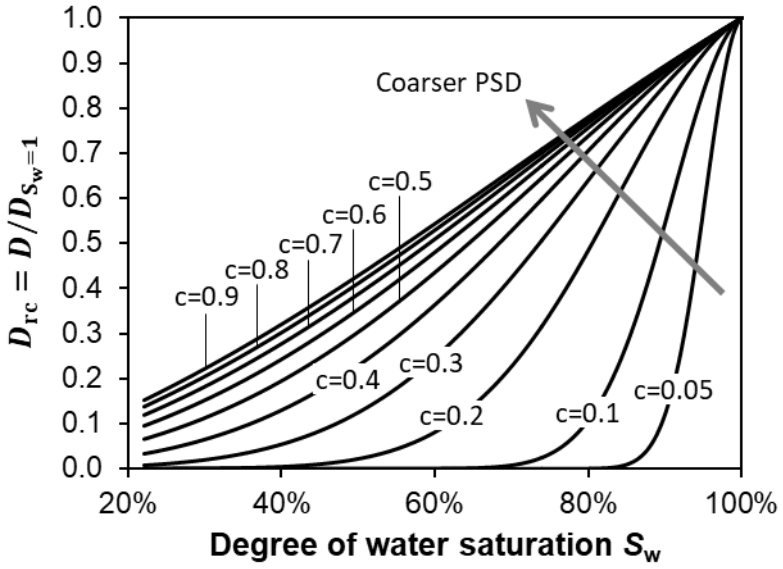

278

279 **Fig. 4.** The D_{rc}-S_w curves calculated by Eq. (15) with the coefficient *c* varying in the range
280 0.05…0.9. A larger *c*-value corresponds to a cementitious material with coarser PSD (pore
281 size distribution)

282

283 **3. Experimental program**

284 3.1. Materials and samples

285 Cement paste and mortar samples were prepared. The mixture proportions for the binders are
286 listed in Table 1. The mixtures were designed with the considerations of varying water-to-
287 binder (w/b) ratios (0.4, 0.5 and 0.6) and different binder materials. The binders used in the
288 experimental program were ordinary Portland cement (OPC) and supplementary cementitious
289 materials (SCMs), including fly ash (FA), limestone powder (LP) and ground granulated blast
290 furnace slag (BFS). The amount of SCMs in the binders was chosen according to the different
291 types of cement, for example, CEM II/B-M with 30% of FA and CEM III/B with 70% of

BFS. All mortar samples were made with the same amount of siliceous sand. The particle size of the siliceous sand ranged from 0.125 to 2 mm. Both paste and mortar samples were cured at 20±0.1 ˚C for one year.

Table 1 Mixture proportions of the binders used for paste and mortar samples

Mixtures	Types of cement	Raw materials by weight				W/b
		OPC	FA	BFS	LP	
M4	CEM I	100%	-	-	-	0.4
M5	CEM I	100%	-	-	-	0.5
M6	CEM I	100%	-	-	-	0.6
MF5	CEM II/B-M	70%	30%	-	-	0.5
MB5	CEM III/B	30%	-	70%	-	0.5
MBL5	-	25%	-	70%	5%	0.5

For pore structure analysis, the one-year-old paste samples were crushed into small pieces (around 1 cm^3). The crushed samples were immersed in liquid nitrogen at -195 ˚C for 5 minutes, and then placed in a freeze-dryer with -24 ˚C and under vacuum at 0.1 Pa. After the water loss was below 0.01% per day, the dried paste samples were ready for pore structure measurements.

Part of the mortar samples was used for resistivity measurements and the rest for pore solution chemistry measurements. For resistivity measurements, the one-year-old mortar samples (ϕ100 × 50 mm) were preconditioned in an oven at 50 ˚C to reach uniform moisture content with the S_w ranging from 18 to 100%. The details of the sample preconditioning procedures in obtaining uniform moisture content can be found in previous work [28]. Note

307 that the samples after the preconditioning had very dry surfaces. This effect was assumed
308 negligible in this experimental study. The pore solutions were extracted from one-year moist-
309 cured mortars (ϕ50 × 100 mm) according to the pore solution expression method provided by
310 Barneyback and Diamond [31]. The extracted pore solutions were filtered using a 0.45 μm
311 pore size filter to remove the possible residual particles. The filtered pore solutions were
312 ready for chemistry measurements.

313 3.2. Pore structure measurement

314 The pore structure measurements were performed by mercury intrusion porosimetry (MIP)
315 technique. The intruding pore diameter d [μm] at pressure P [MPa] was determined by the
316 Washburn equation [32]:

$$d = -\frac{4\gamma_{\mathrm{Hg}}\, cos\, \theta}{P} \tag{16}$$

317 where γ_{Hg} is the surface tension of mercury (0.48 kN/m); θ is the contact angle between
318 mercury and pore wall of the specimen (139˚).

319 For a given porous system the average pore diameter d_{a} is defined as [30]:

$$d_{\mathrm{a}} = \frac{4V_{\mathrm{t}}}{S_{\mathrm{t}}} \tag{17}$$

320 where V_{t} [m^3/m^3] and S_{t} [m^2/m^3] are the total pore volume and the total pore surface area,
321 respectively. In principle the smaller pores have a lower volume-surface area ratio. A smaller
322 average pore diameter d_{a} accounts for a finer pore size distribution. In the sense that the pore

size distribution significantly influences the moisture distribution, the average pore diameter can be very effective to indicate the water continuity and unsaturated ionic transport.

3.3. Resistivity measurement

Electrical resistivity measurements were carried out on mortar specimens preconditioned with uniform moisture content (S_w = 18~100%). The principles of the resistivity measurements can be referred to Refs. [23, 28]. The electrical resistance R of each mortar specimen was measured with one stainless steel electrode covering each side of the specimen. A wet sponge was applied between specimen surface and each electrode to ensure the whole surface of the specimen under current flow. During the test, the measured resistance R was found to gradually decrease with time. This can be attributed to the moisture transfer from the wet sponge into the specimen. To minimize this effect, only the resistance result obtained from the first measurement was adopted. The resistivities (ρ-values), as well as the conductivities (σ_{S_w}-values), of the mortar specimens tested were calculated as a function of the measured resistances R by using Eq. (5).

3.4. Pore solution chemistry and its conductivity

The initial pore solutions in various mortar specimens at saturated state (S_w = 100%) were squeezed out (according to pore expression method [31]), collected, filtered, and then measured by means of inductively coupled plasma optical emission spectrometry (ICP-OES). The concentrations of alkalis (Na^+, K^+) were derived. The concentration of OH^- was computed as the sum of the concentrations of the alkalis (Na^+, K^+) [33].

A decrease of the degree of water saturation S_w results in a *non-linear* increase of the alkali concentrations, because of the non-linear binding isotherm of the alkalis (Na^+, K^+) in cementitious materials. The alkalis (Na^+, K^+) released during hydration are either bound by hydrates (mainly C-S-H) or present as free ions in the pore solution. Chen and Brouwers [34] have proposed a method for determining the relationship between bound and free alkalis contents. The method was extended in this work, as indicated in Eqs. (18) and (19), to predict the alkali concentrations at different degrees of water saturation S_w.

$$C_{\mathrm{Na}} = \frac{n_{\mathrm{Na}}^{\mathrm{r}}}{\phi_{\mathrm{t}} \cdot S_{\mathrm{w}} + Rd \cdot m_{\mathrm{C-S-H}}} \tag{18}$$

$$C_{\mathrm{K}} \cdot \phi_{\mathrm{t}} \cdot S_{\mathrm{w}} + K_{\mathrm{f}} \cdot (C_{\mathrm{K}})^{0.24} \cdot m_{\mathrm{C-S-H}} = n_{\mathrm{K}}^{\mathrm{r}} \tag{19}$$

Various parameters are described as follows:

a) Rd is the distribution ratio (Rd = 0.45×10^{-3} L/g); K_f is the adsorption coefficient (K_f = 0.20×10^{-3} L/g); ϕ_t is the total porosity of the mortar specimen; S_w is the degree of water saturation. The total porosity ϕ_t of the mortar specimen was determined following the recommendation of ASTM C642-13 [35].

b) m_{C-S-H} [g] is the mass of C-S-H, which is simplified as the composition of $C_{1.7}SH_4$ for OPC binder and as $C_{1.5}SH_{3.8}$ for blended binders (MF5, MB5 and MBL5) [36]. The value of m_{C-S-H} was estimated by Thermogravimetric analysis (TGA/DSC) with the assumption that the released water was from the thermal decomposition of C-S-H (105~1100 ˚C) and calcium hydroxide (400~550 ˚C) [37].

c) C_{Na} and C_K [mol/L] represent the concentration of Na^+ and K^+, respectively.

d) n_{Na}^r and n_K^r refer to the moles of alkalis Na^+ and K^+ released during hydration. At S_w = 100%, C_{Na} and C_K were measured from ICP-OES. Substituting the values of the

parameters (ϕ_t, m_{C-S-H}, C_{Na} and C_K) into Eqs. (18) and (19) determines the values of n_{Na}^r and n_K^r.

The parameters (n_{Na}^r, n_K^r, ϕ_t and m_{C-S-H}) are considered constant for a given mortar mixture. Hence, the alkali concentrations C_{Na} and C_K in the pore solution of each mortar at various saturation levels (S_w < 100%) can be predicted with Eqs. (18) and (19). Then synthetic solutions were prepared by mixing the solids NaOH and KOH with distilled water in proper proportions to achieve the same chemical compositions as the concentrations of the ions Na^+, K^+ and OH^- at each saturation level S_w. The conductivities of the pore solution at various saturation levels, viz. σ_{p,S_w}-values, were obtained from conductivity tests performed on these synthetic solutions.

4. Experimental results

4.1. Conductivity of pore solution at various degrees of water saturation

The concentrations of ions (Na^+, K^+ and OH^-) as a function of the degree of water saturation S_w were calculated. The results of two mortars M5 (OPC) and MF5 (FA 30%), as an example, are shown in Fig. 5a. For a given saturation level S_w, the concentration of each ion species (Na^+, K^+ or OH^-) in the blended mortar MF5 is lower than that in the reference OPC mortar M5. The concentration of K^+ is normally higher than that of Na^+ in both mortars M5 and MF5. This phenomenon is particularly obvious at low saturation levels, i.e. S_w < 60%.

Figure 5b gives the measured conductivity σ_p of the synthetic pore solution at different saturation levels S_w for six mortar mixtures. Compared to the OPC mortar M5, the mortars blended with SCMs (FA, BFS or LP) generally show lower conductivity σ_p of pore solution

in the entire saturation range. For any given saturation level S_w, the conductivity σ_p of the pore solution in mortar MB5 (BFS 70%) is approximately half that in mortar MF5 (FA 30%). The σ_p-value non-linearly increases with decreasing saturation level S_w. Especially for S_w < 60%, a relatively rapid increase of the σ_p-value is observed as the S_w further decreases. The σ_p-value is almost doubled when the S_w decreases from 100 to 30%, regardless of the w/b ratio or the binder type.

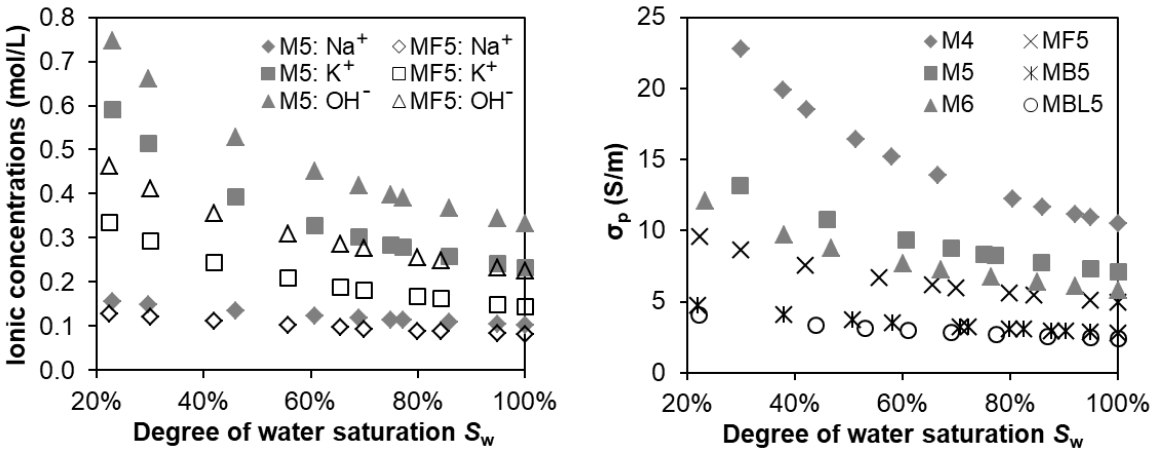

(a) (b)

Fig. 5. (a) Ionic concentrations as a function of saturation level S_w in mortars M5 and MF5; (b) Measured conductivity σ_p of synthetic pore solution at different saturation levels S_w. Mortar mixtures: M4 (OPC, w/b = 0.4), M5 (OPC, w/b = 0.5), M6 (OPC, w/b = 0.6), MF5 (FA 30%, w/b = 0.5), MB5 (BFS 70%, w/b = 0.5), MBL5 (BFS 70% + LP 5%, w/b = 0.5). The σ_p-S_w plots of OPC mortars (M4, M5 and M6) were presented in previous work [28]

Note that the σ_p-values shown in Fig. 5b were determined based on conductivity tests performed on synthetic aqueous solutions. In case these aqueous solutions were present in the pore structure of mortar specimens, with pore-scale from several nanometers to several

402 micrometers, the measured σ_p-values may differ. Such differences are briefly evaluated in the
403 following.

404 It is well-known that when an aqueous electrolyte meets a solid, the solid surface will be
405 charged because of physical adsorptions and/or chemical reactions [38]. The surface charge
406 will induce an electrical double layer (EDL) near the solid surface and, as a consequence,
407 affecting the ionic distribution in the pore structure and conductivity of the pore solution [39].
408 The EDL effect on the conductivity σ_p of the pore solution is negligible when the pore size is
409 sufficiently large compared with the thickness of the EDL, but becomes increasingly
410 pronounced with a decrease of the pore size, particularly for the pore diameter smaller than
411 10 nm [39, 40]. From a case study on saturated CEM-V paste, with the pores below 10 nm in
412 diameter constituting about 60% of the total pore volume as estimated from MIP tests, the
413 electrical conductivity considering the EDL effect was found to be around 1.2 times that
414 neglecting the EDL effect [40]. The case study provides a reference for examining the
415 deviation of the measured σ_p-values (Fig. 5b) from the actual σ_p-values of the pore solutions.

416 The pore size distributions of the paste specimens used in the present work (Table 1) were
417 identified by MIP tests. The volume of the pores (diameter < 10 nm), normalized to the total
418 pore volume, is less than 15% for mixtures (M4, M5, M6 and MF5), less than 22% for
419 mixture MBL5, and less than 50% for mixture MB5. In comparison with the case study
420 abovementioned [40], the measured σ_p-values given in Fig. 5b can be reasonably considered
421 as the conductivities of the pore solutions present in the unsaturated specimens M4, M5, M6
422 and MF5. This consideration is valid even for the low saturation levels. Take mixture MF5
423 for example, at S_w = 25%, the volume of the water-filled pores (with diameter < 10 nm)
424 determined from MIP-derived pore size distribution accounts for around 60% of the total

425 volume of water-filled pores. This will result in the measured σ_p-value at S_w = 25% (Fig. 5b)
426 to be merely 1.2 times smaller than the actual σ_p-value of the pore solution at S_w = 25%. Such
427 1.2 times of discrepancy will be achieved for mixture MBL5 with S_w as low as 36%, whereas
428 for mixture MB5 at S_w = 80%. Accordingly, for mixture MB5 the measured σ_p-values (Fig.
429 5b) are considered to deviate the actual σ_p-values of the pore solutions more than 1.2 times
430 when the S_w is lower than 80%. Additional research work can be done to obtain more precise
431 σ_p-values of the pore solutions in the slag-blended mixture MB5 at S_w < 80%.

432 4.2. Relative chloride diffusion coefficient at various degrees of water saturation

433 The conductivities of both cementitious mortars and their synthetic pore solutions were
434 measured. By using Eq. (13), the relative chloride diffusion coefficient D_{rc} was determined as
435 a function of the degree of water saturation S_w.

436 Figure 6a shows the D_{rc}-S_w plots in the OPC mortars with w/b ratios of 0.4, 0.5 and 0.6.
437 There is a general trend that the D_{rc} decreases with decreasing saturation level S_w. The most
438 significant decrease of the D_{rc}-value is observed in the high saturation range, i.e. S_w > 60%. It
439 makes sense that a rapid drop of the water continuity has taken place in this high saturation
440 range. Once the S_w is below 60%, the D_{rc}-value is more than one order of magnitude lower
441 than that at saturated state, regardless of the w/b ratio. For more details about the effect of the
442 w/b ratio on the D_{rc}-S_w relation, reference is made to a previous experimental study [28].

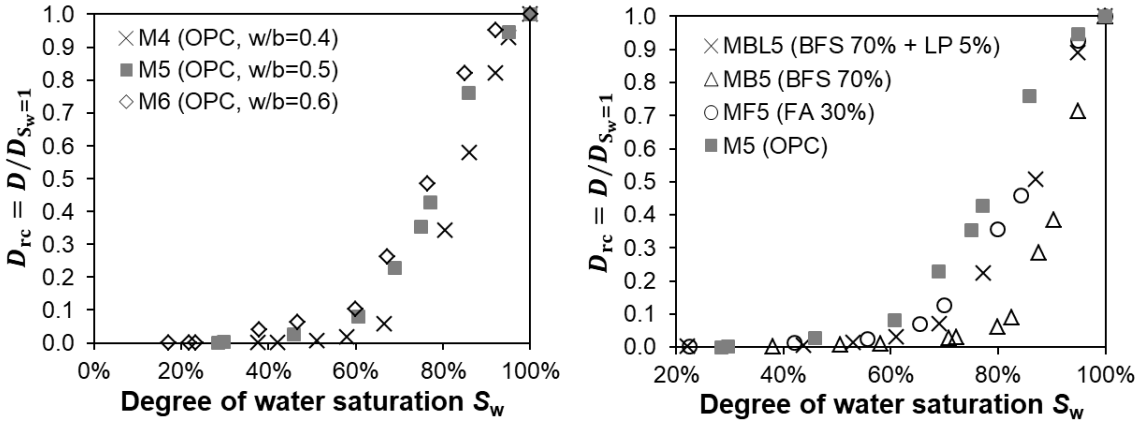

(a) (b)

Fig. 6. Relative chloride diffusion coefficient ($D_{rc}=D/D_{S_w=1}$) as a function of degree of water saturation S_w: (a) one-year-old OPC mortars with w/b ratios of 0.4, 0.5 and 0.6; (b) one-year-old blended mortars with constant w/b ratio of 0.5. The D_{rc}-S_w plots of OPC mortars (M4, M5 and M6) were presented in previous work [28]

Figure 6b shows the effects of SCMs on the D_{rc}-S_w relationship. At a particular saturation level S_w, the mortars containing FA or BFS commonly exhibit lower D_{rc} than the reference OPC mortar M5. For instance, at S_w = 80%, the D_{rc}-value is approximately 0.1 for MB5, 0.3 for MBL5 and 0.35 for MF5, compared to a much higher D_{rc}-value of 0.6 for M5.

5. Validation of the model of relative chloride diffusion coefficient

An analytical model (Eq. (15)) of relative chloride diffusion coefficient has been established. Comparison of the model with experimental data, including data derived in this work and those reported in the literature, is carried out in order to test the reliability and efficiency of the model.

459 5.1. Validation of the model with experimental data derived in this work

460 The D_{rc}-S_w data of OPC mortars, as shown in Fig. 6a, are compared with the model (Eq. (15)).
461 Good agreement is observed in the entire saturation range, regardless of the w/b ratios. The
462 correlation coefficients are 0.997 for specimen M4 (w/b = 0.4), 0.989 for specimen M5 (w/b
463 = 0.5) and 0.973 for specimen M6 (w/b = 0.6). According to regression analyses, the
464 coefficient *c* in Eq. (15) is determined as 0.164, 0.214 and 0.256 for specimens M4, M5 and
465 M6, respectively.

466 Equation (15) is also compared with the existing equations (Eq. (2) and Eq. (3)). The
467 comparison is made by examining the fitness of these equations to the D_{rc}-S_w plots of mortar
468 M5 as presented in Fig. 6a. The fitting curves are given in Fig. 7. It is clear that Eq. (15)
469 shows the best fitness amongst these equations. For the power equation (Eq. (2)), the D_{rc}-
470 value is underestimated at high saturation levels (S_w > 75%) while overestimated at low
471 saturation levels (S_w < 75%). At S_w < 40%, Eq. (2) is found to overestimate the D_{rc}-value
472 more than one order of magnitude. For the polynomial equation (Eq. (3)), the D_{rc}-value is
473 also underestimated at high saturation levels (S_w > 75%). The D_{rc}-value is fitted as zero at S_w
474 = 46%, inferring that Eq. (3) becomes ineffective to predict the D_{rc} at lower saturation levels,
475 i.e. S_w < 46%.

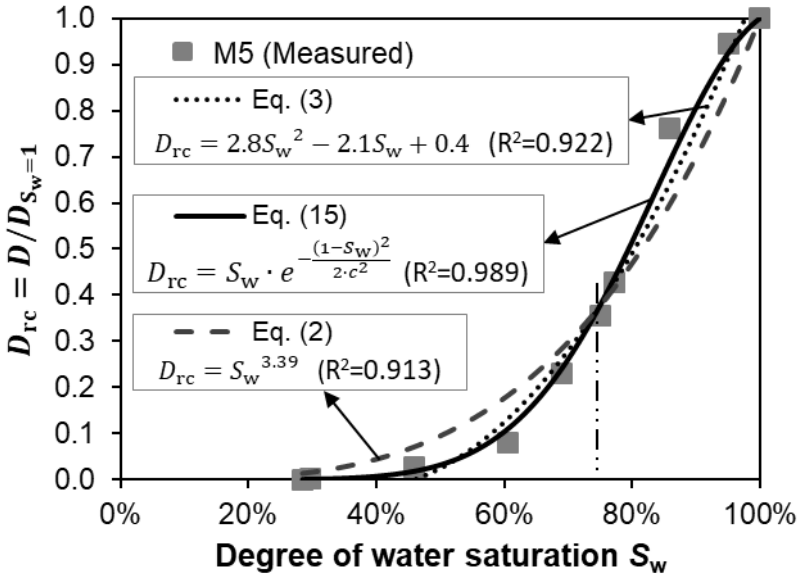

476

477 **Fig. 7.** Comparison of different equations based on their fitness to the measured D_{rc}-S_w plots

478 of mortar M5 as presented in Fig. 6a

479

480 Comparison of Eq. (15) with the D_{rc}-S_w data presented in Fig. 6b is further performed. The

481 regression curves are given in Fig. 8. Good agreement between experimental D_{rc}-S_w data and

482 Eq. (15) is observed for all binders studied. The correlation coefficients are 0.997, 0.992 and

483 0.997 for mortars MF5, MB5 and MBL5, respectively. From the curve-fittings, the

484 coefficient *c* in Eq. (15) is determined as 0.154, 0.077 and 0.135 for mortars MF5, MB5 and

485 MBL5, respectively.

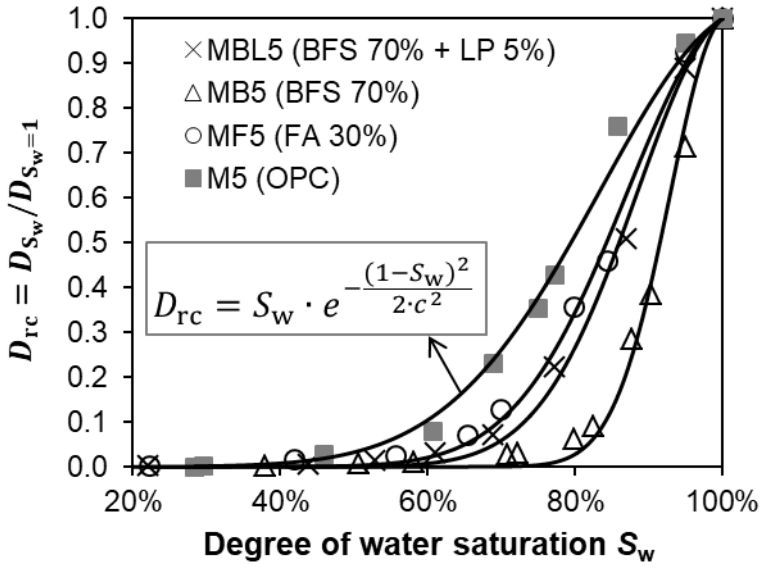

Fig. 8. Regression curves (D_{rc} *vs.* S_w) obtained by using Eq. (15) to fit the experimental data presented in Fig. 6b

5.2. Validation of the model with experimental data reported in the literature

A series of previously published D_{rc}-S_w data and details of the experiments are provided in Fig. 9 and Table 2, respectively. These D_{rc}-S_w data were obtained based on the Nernst-Einstein equation and conductivity measurements. Since the information of the pore size distribution of the specimens is not available in these studies [13, 17, 41, 42], the porosities of the specimens are given instead.

From Fig. 9, high correlation coefficients (R^2) are observed. It is clear that Eq. (15) describes these data series (D_{rc} *vs.* S_w) quite well, regardless of binder type, w/b ratio or porosity of the specimens. A direct relationship between porosity and D_{rc}-S_w relation cannot be obtained. For a given saturation level S_w the lower D_{rc}-value, as shown in Fig. 9, should be attributed to a finer pore size distribution in the specimen.

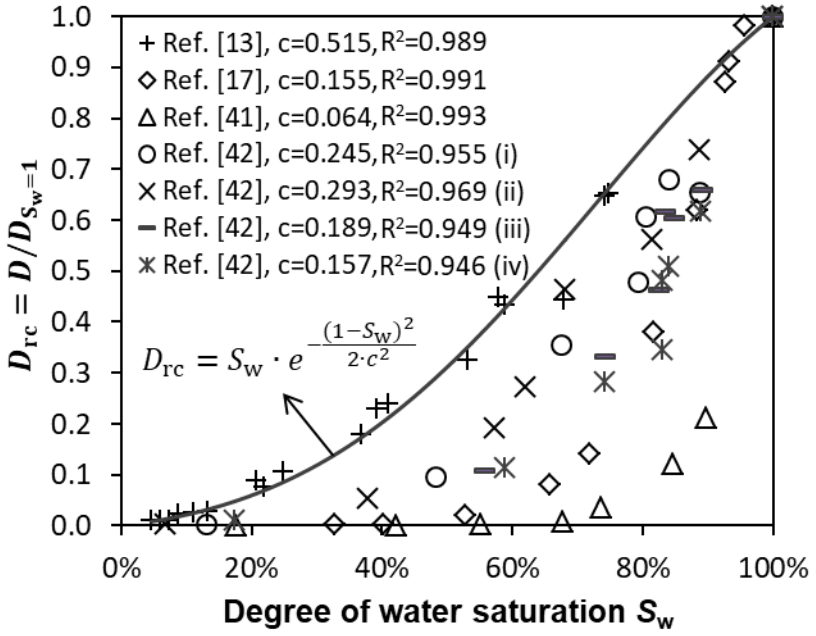

501

502 **Fig. 9.** Calibration of Eq. (15) with experimental D_{rc}-S_w data reported in literature. The values

503 of coefficient *c* and correlation coefficient R^2 are obtained from regression analyses

504

505 Table 2 Previous experimental studies about relative chloride diffusion coefficient

Authors	Binder type	Specimen	W/b	Porosity
Buchwald [13]		Masonry materials		32%
Rajabipour [17]	ASTM Type I	Concrete (18 months)	0.50	17.7%
Mercado-Mendoza et al. [41]	CEM V (55% OPC + 22% Slag + 23% Fly ash)	Concrete (6 months)	0.41	14%
Olsson et al. [42]	(i) OPC	Mortar (3 months)	0.38	15%
Olsson et al. [42]	(ii) 95% OPC + 5% Silica fume	Mortar (3 months)	0.531	19%
Olsson et al. [42]	(iii) 60% OPC + 40% Slag	Mortar (3 months)	0.386	16%
Olsson et al. [42]	(iii) 30% OPC + 70% Slag	Mortar (3 months)	0.391	16%

506

507 5.3. Determination of the coefficient *c* and prediction of the relative chloride diffusion
508 coefficient

509 As proved in Sections 5.1 and 5.2, the analytical model (Eq. (15)) agrees fairly well with the
510 experimental D_{rc}-S_w data. Prediction of the relative chloride diffusion coefficient D_{rc} with Eq.
511 (15) is possible once the coefficient *c* of the material under study is known. As noted earlier,
512 the coefficient *c* is related to the fineness of the pore size distribution in the specimen. In the
513 case when the average pore diameter d_a (defined by Eq. (17)) is adopted to indicate the
514 fineness of pore size, the *c*-value shall then be described as a function of the average pore
515 diameter, i.e. $c = c(d_a)$.

516 Calibration of Eq. (15) with the experimental data shown in Fig. 6a-b yielded the *c* values for
517 different mixtures. The average pore diameter d_a of these mixtures was determined according
518 to the pore size distribution of paste specimens derived from MIP measurements. Figure 10
519 depicts the coefficient *c* versus average pore diameter d_a for all mixtures studied. A linear
520 relationship (Eq. (20)) with a correlation coefficient of 0.92 is found.

$$c(d_a) = k_1 \cdot d_a + k_2 \qquad (R^2 = 0.92) \tag{20}$$

521 where k_1 [nm^{-1}] and k_2 [-] are constants. Both depend on the pore structure of the materials.
522 The regression analysis shown in Fig. 10 gives that $k_1 = 0.01$ and $k_2 = -0.05$.

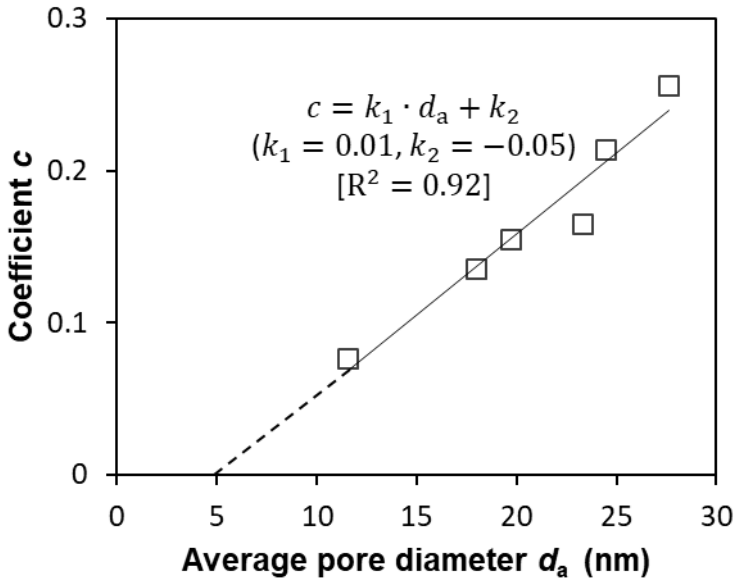

Fig. 10. Relationship between coefficient c and average pore diameter d_a

The linear trend (Fig. 10) shows that the coefficient c approaches zero at $d_a \approx 5$ nm. Both η_w (Eq. (11)) and D_{rc} (Eq. (15)) are then determined as zero at $d_a \leq 5$ nm. This is reasonable against the background of the microstructure of cementitious materials. At $d_a > 5$ nm, the microstructure contains both capillary pores (> 10 nm) and gel pores (≤ 10 nm). Whereas at $d_a \leq 5$ nm, there may be little capillary pores but only gel pores present in the microstructure and hence the chloride diffusion is negligible [43]. For hydrated cementitious materials (> 28 days old) the average pore diameter d_a rarely exceeds 50 nm [44] and, therefore, the c-value is usually in the range 0~0.45.

The linear equation (Eq. (20)) allows the water continuity η_w (Eq. (11)) to be described as a function of the degree of water saturation S_w and the pore structure (indicated by average pore diameter d_a).

$$\eta_{\mathrm{w}} = e^{-\frac{(1-S_{\mathrm{w}})^2}{2\cdot(0.01d_{\mathrm{a}}-0.05)^2}} \qquad (d_{\mathrm{a}} > 5\ nm) \qquad (21)$$

Consequently, Eq. (15) is extended and the relative chloride diffusion coefficient D_{rc} in unsaturated cementitious materials can be predicted as:

$$D_{\mathrm{rc}} = \frac{D_{\mathrm{S_w}}}{D_{\mathrm{Sat}}} = S_{\mathrm{w}} \cdot e^{-\frac{(1-S_{\mathrm{w}})^2}{2\cdot(0.01d_{\mathrm{a}}-0.05)^2}} \qquad (d_{\mathrm{a}} > 5\ nm) \qquad (22a)$$

$$D_{\mathrm{rc}} = 0 \qquad (d_{\mathrm{a}} \leq 5\ nm) \qquad (22b)$$

where $D_{\mathrm{S_w}}$ [m^2/s] is the chloride diffusion coefficient at a particular degree of water saturation S_{w} [-]; D_{Sat} [m^2/s] is the chloride diffusion coefficient at saturated state, which can be obtained from resistivity measurements, steady-state diffusion or migration cell methods [19]; d_{a} [nm] is the average pore diameter of the material estimated from MIP test.

The linear relationship (Eq. (20)) was derived based on the *c*-d_{a} plots of six mixtures, covering different w/b ratios (0.4~0.6) and cementing types (OPC, FA, BFS and LP). It is worthwhile to point out that natural and artificial blended materials have nowadays been widely used to partially or even entirely replace the OPC for hydraulic binders. More experimental investigations can be conducted to examine whether the equation (Eq. (20)), as well as the analytical model (Eq. (22a) and Eq. (22b)), is applicable for other hydraulic binders. Improvement to Eq. (22a) and Eq. (22b), such as using a more effective relationship between the coefficient *c* and the microstructure information, is possible.

6. Discussion

An analytical model (Eq. (22a) and Eq. (22b)) has been established, with which the chloride diffusion coefficient D_{S_w} at unsaturated state can be predicted based on the chloride diffusion coefficient D_{Sat} at saturated state, the degree of water saturation S_w and the average pore diameter d_a of the material.

We intend to proceed with a detailed discussion on the model (Eq. (22a) and Eq. (22b)) in order to facilitate its implementation into engineering practice. Two aspects will be discussed in the following.

6.1. Whether the D_{rc}-S_w relation is constant for a given cementitious material?

For a given cementitious material the D_{rc}-S_w relation is dependent on the moisture distribution [28, 45]. In the case of *idealized* moisture distribution, the water phase fills a pore system from small pores to larger pores and, therefore, the moisture distribution in the pore system is expected to be constant at a specific saturation level S_w. However, the idealized moisture distribution hardly exists for onsite cementitious materials, in which repeated water desorption-absorption cycles often take place before an equilibrium moisture state is achieved. A desorption-absorption cycle can result in moisture hysteresis because of the pore constriction in cementitious materials, as schematically illustrated in Fig. 11.

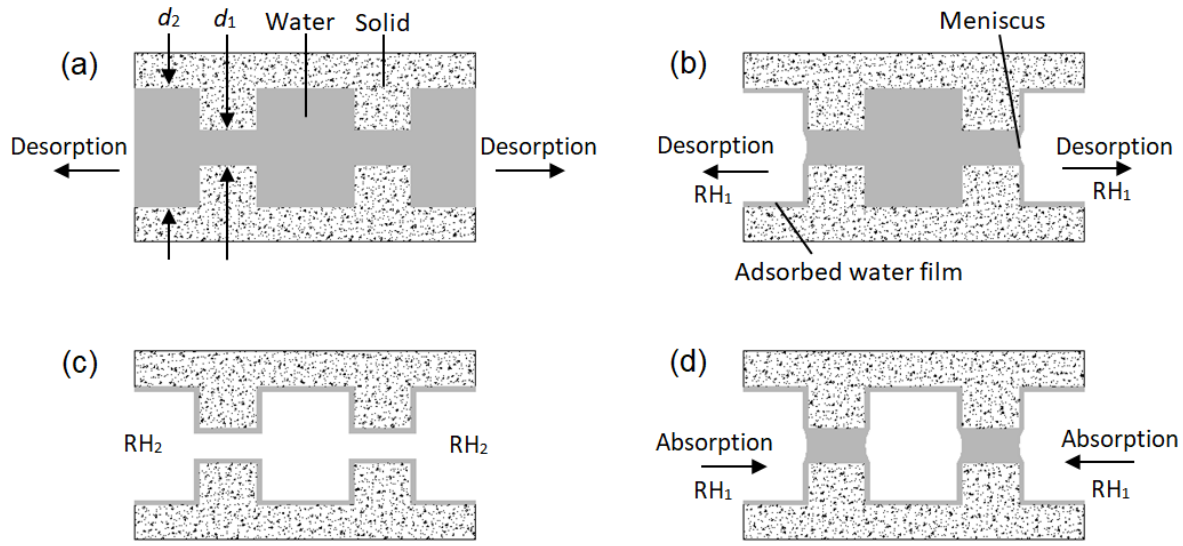

Fig. 11. Moisture hysteresis in a desorption-absorption cycle under isothermal condition: (a) saturated; (b) desorption to RH_1; (c) further desorption to RH_2; (D) absorption to RH_1

Figure 11a shows a channel consisting of small pores (diameter d_1) and large pores (diameter d_2). The channel is initially saturated with water. Figure 11b shows water desorption from saturated state to RH_1, the large pores d_2 at the two ends are drained (only an adsorbed water film is present). Figure 11c shows further desorption from RH_1 to RH_2 ($RH_2 < RH_1$). The whole channel is drained. Figure 11d shows an *absorption* process from RH_2 to RH_1. The throat pores d_1 are fully filled with water while in the ink-bottle pores d_2 only an adsorbed water film is present. With the same RH_1 level the water contents present in Fig. 11b and Fig. 11d are different. This in turn reveals that at a specific degree of water saturation S_w the internal RH of a given porous system can be different and, moreover, the distribution of water-filled pores (controlled by internal RH via the Kelvin law) and their continuity (i.e. water continuity η_w) can be different as well. It is sensible to conclude, therefore, that for a given cementitious material the relationship between relative chloride diffusion coefficient

584 D_{rc} and moisture content (indicated by either S_w or RH) is not constant, but depends on the
585 dynamic moisture loading history of the material.

586 For a further examination of the D_{rc}-S_w relationship, a schematic representation of a sorption
587 isotherm in cementitious materials is presented in Fig. 12, where the *absorption* and
588 *desorption* curves are plotted based on a literature survey [46, 47]. It is clear that a given
589 saturation level S_{w1} corresponds to two humidity levels: RH_1 referring to the minimum
590 humidity level obtained from desorption isotherm and RH_2 referring to the maximum
591 humidity level obtained from absorption isotherm. The two humidity levels, RH_1 and RH_2,
592 are expected to result in the minimum and the maximum d_p-value (d_p is the smallest drained
593 pore diameter following the Kelvin-Cohen equation [29]), and hence the minimum and the
594 maximum water continuity η_w, respectively.

595 In the present work the water continuity η_w and associated relative chloride diffusion
596 coefficient D_{rc} were determined based on the moisture distribution estimated from desorption
597 isotherm. The chloride diffusion coefficient D_{S_w} predicted from the model (Eq. (22a)) is
598 therefore considered the minimum value achievable at a particular saturation level S_w. The
599 maximum D_{S_w} value achievable at this saturation level S_w can be predicted from the
600 knowledge of the moisture distribution estimated from absorption isotherm.

601 In engineering practice, it is not easy to precisely capture the dynamic moisture loading
602 history of onsite concretes. For a given concrete in equilibrium moisture state, the D_{rc}-S_w
603 relation is not constant but variably situated in the shadow zone, as indicated in Fig. 13.

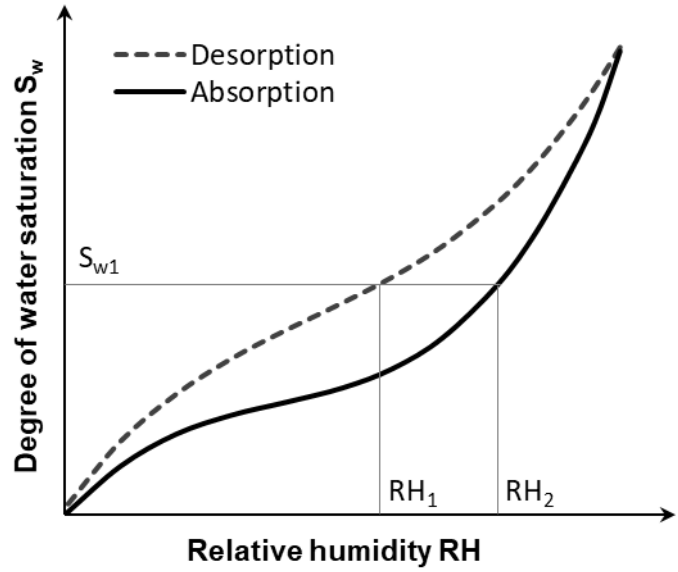

604

605 **Fig. 12.** Schematic representation of a sorption isotherm with hysteresis between absorption

606 and desorption isotherms in cementitious materials under isothermal condition

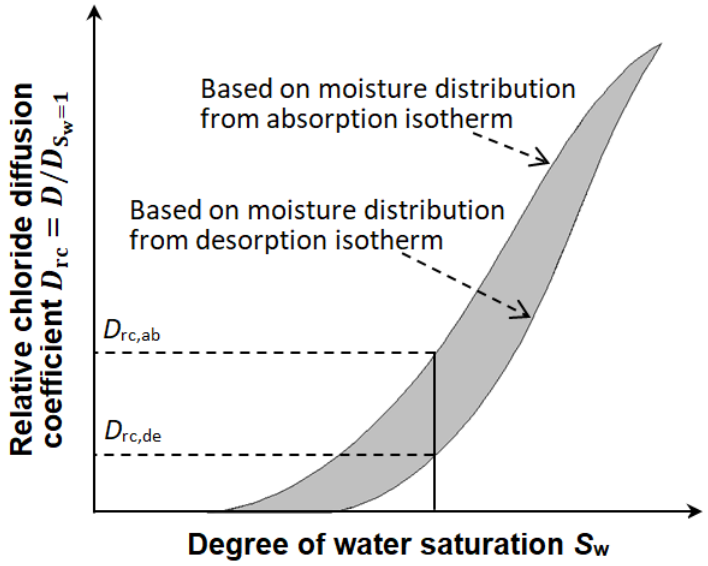

607

608 **Fig. 13.** Schematic illustrations of the D_{rc}-S_w relations based on the moisture distributions

609 from desorption and absorption isotherms. For an unsaturated cementitious material with

610 unknown moisture loading history, the D_{rc}-value at a given saturation level S_w is predicted in

611 the range from $D_{rc,de}$ to $D_{rc,ab}$

612

6.2. To what extent can pore structure affect D_{rc}-S_w relation?

The role of the pore structure in the D_{rc}-S_w relation is mainly a result of its effect on the water continuity. A finer pore size distribution tends to result in a lower water continuity and hence a lower D_{rc}-value. The average pore diameter d_a (Eq. (17)) has been introduced to indicate the fineness of pore size. To what extent can the pore structure (indicated by the average pore diameter d_a) influence the D_{rc}-S_w relation, a detailed discussion is presented.

The changes of the D_{rc} with increasing d_a from 10 to 200 nm for different saturation levels S_w are shown in Fig. 14, where the curves were calculated by Eq. (22a). A similar tendency can be found for the D_{rc}-d_a curves at different saturation levels (S_w = 10~95%). For a given S_w the D_{rc} is influenced by the d_a only when the d_a value is small. The D_{rc}-value tends to reach a constant (equal to the S_w-value) once the d_a is sufficiently large. This observation is reasonable in view of the pore structure characteristics of cementitious materials. In general, a larger d_a corresponds to a more porous pore network. For a pore structure with the d_a large enough, all the pores are considered well connected and the whole pore network can then be treated as one big channel. As a consequence, the D_{rc} tends to linearly decrease with the decreasing amount of water available for ionic transport, i.e. linear D_{rc}-S_w relationship is expected as can be deduced from Eq. (22a) at $d_a \rightarrow \infty$.

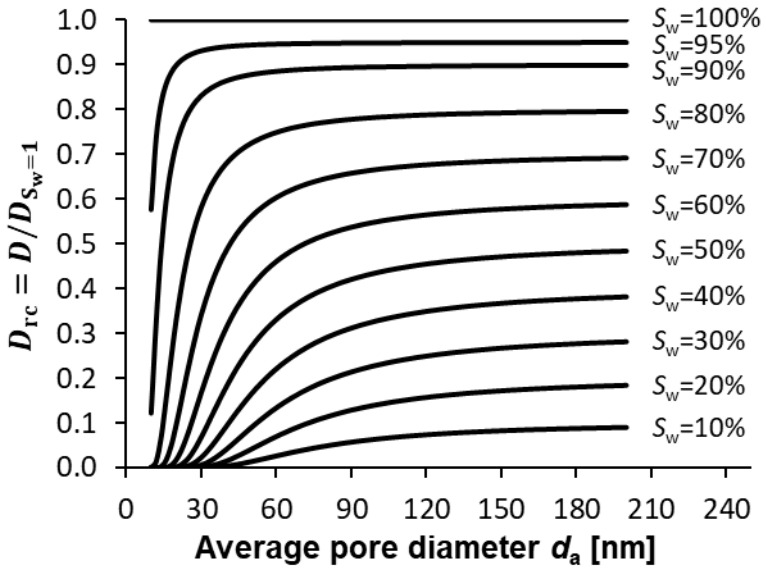

630

631 **Fig. 14.** Influences of pore structure (indicated by average pore diameter d_a: 10~200 nm) on
632 the relative chloride diffusion coefficient D_{rc} at different degrees of water saturation S_w

633

634 Besides, the D_{rc}-d_a curves show differences for different saturation levels S_w.

635 ▪ At saturated state (S_w = 100%), the D_{rc} is equal to one, independent of the d_a. In other
636 words, the pore structure has no influence on the D_{rc} at S_w = 100%. There is no doubt
637 in this point based on the definition of the D_{rc}.

638 ▪ At S_w = 95%, the most rapid change of the D_{rc} occurs when the d_a increases from 10
639 to 15 nm. Less rapid but clearly distinguishable change of the D_{rc} is observed until the
640 d_a further increases up to 30 nm, after which the D_{rc} changes little. It is revealed that
641 when the S_w is as high as 95% the D_{rc} will be influenced by the pore structure only if
642 $d_a \leq 30$ nm. For pore structures with $d_a > 30$ nm, the D_{rc} tends to be a constant
643 (approaching 0.95).

644 ▪ A remarkable decrease of the D_{rc} at d_a = 10 nm is observed when the S_w decreases
645 from 95% (D_{rc} = 0.58) to 90% (D_{rc} = 0.12). For S_w = 90%, a slight increase of the d_a
646 leads to a steep jump of the D_{rc} until the d_a reaches approximately 30 nm, after which

the increase of the D_{rc} is less significant. The D_{rc} changes slightly at d_a > 40 nm, and nearly reaches a constant at d_a > 50 nm. For S_w = 80%, the D_{rc} suddenly drops to almost zero at d_a = 10 nm and the increase of the D_{rc} with increasing d_a becomes less pronounced, compared to the cases for S_w = 90% and S_w = 95%. For S_w = 80%, a slight slow change of the D_{rc} is observed at d_a > 50 nm and the D_{rc} is nearly unchanged at d_a > 80 nm.

- A further decrease of the S_w results in the D_{rc} to be less influenced by the d_a. For example, at S_w = 40%, the D_{rc} increases merely from 0 to 0.32 when the d_a increases greatly from 10 to 100 nm. When the S_w approaches zero the D_{rc} is expected to be infinitely small, regardless of the d_a.

The foregoing discussion enables to partition the dependency of the D_{rc}-S_w relation on the pore structure in accordance to the value of the average pore diameter d_a:

1) At $d_a \leq 30$ nm, the pore structure significantly influences the D_{rc} in the wide saturation range $10\% \leq S_w \leq 95\%$.
2) At 30 nm < $d_a \leq 50$ nm, the pore structure has a minor influence on the D_{rc} for high saturation range ($S_w \geq 90\%$), but has a great influence on the D_{rc} for $S_w \leq 80\%$.
3) At 50 nm < $d_a \leq 100$ nm, the pore structure has a minor influence on the D_{rc} for $S_w \geq 80\%$, but still exhibits an obvious influence on the D_{rc} for $S_w \leq 70\%$.
4) At d_a > 100 nm, the influence of the pore structure on the D_{rc} is negligible for $S_w \geq 60\%$, which is a common saturation range in cementitious materials.

A number of systematically experimental studies [44, 48] have shown that the average pore diameter d_a of well-cured cementitious materials (> 28 days old) is normally below 50 nm. It is therefore considered that the pore structure can play an important role in the D_{rc}-S_w relation of hydrated cementitious materials.

7. Summary and concluding remarks

In the present work an analytical model (Eq. (15)) has been developed, with which the *relative chloride diffusion coefficient* D_{rc} is described as a function of the degree of water saturation S_w. The model takes the moisture distribution into account. The model has been verified with experimental data derived in this work and with those reported in the literature as well.

Equation (15) is extended into Eq. (22a) and Eq. (22b) according to the experimentally obtained linear relationship between the coefficient c and the average pore diameter d_a in cementitious materials. The model (Eq. (22a) and Eq. (22b)) allows predicting the chloride diffusion coefficient D_{S_w} at unsaturated state based on the chloride diffusion coefficient D_{Sat} at saturated state, the degree of water saturation S_w and the average pore diameter d_a of the material. The pore structure with small average pore diameter (d_a < 30 nm) has a significant influence on the D_{rc}-S_w relationship, while the pore structure with large average pore diameter (d_a > 100 nm) has little influence on the D_{rc}-S_w relationship. Herein, the d_a value is identified from MIP measurements.

The water continuity (η_w = 0~1) governs the D_{rc}-S_w relationship. The water continuity η_w depends on the sorption isotherm (including both desorption and absorption isotherms). The sorption isotherm is influenced by pore size distribution and pore constriction. For a given cementitious material the D_{rc}-S_w relation is not constant, but depends on the dynamic moisture loading history.

The modeling of the D_{rc}-S_w relation presented in this work is in a stage of development. Even in this stage, however, the present work helps to understand the mechanisms of unsaturated

chloride diffusion. Moreover, the model (Eq. (22a) and Eq. (22b)) enables to predict the minimum D_{rc} value achievable at any particular saturation level S_w. The maximum D_{rc} value achievable at a given S_w will be determined in the next stage based on the moisture distribution estimated from absorption isotherm. With the help of the model (Eq. (22a) and Eq. (22b)), it is possible to perform mixture design based on the chloride diffusion coefficient of *unsaturated* concrete. This is more reliable than the current mixture design method that is based on the chloride diffusion coefficient of *saturated* concrete.

Acknowledgements

This work has been done under the cooperative framework between Delft University of Technology and South China University of Technology. Funding from the China Scholarship Council (CSC) is gratefully acknowledged. Insightful comments from Prof. Klaas van Breugel are highly appreciated.

References

[1] DuraCrete R17, DuraCrete Final Technical Report, The European Union – Brite EuRam III, DuraCrete – Probabilistic Performance based Durability Design of Concrete Structures, Document BE95-1347/R17, May 2000, CUR, Gouda, The Netherlands.

[2] ACI Committee 365, Service life prediction—state-of-the-art report, Manual of Concrete Practice, ACI 365.1R-00-44, 2001.

[3] H. Justnes, M.O. Kim, S. Ng, X. Qian, Methodology of calculating required chloride diffusion coefficient for intended service life as function of concrete cover in reinforced marine structures, Cem. Concr. Compos. 73 (2016) 316-323.

[4] B. Persson, Moisture in concrete subjected to different kinds of curing, Mater. Struct. 30 (1997) 533-544.

[5] S. Chatterji, An explanation for the unsaturated state of water stored concrete, Cem. Concr. Compos. 26 (2004) 75-79.

[6] J. Zhang, Y. Gao, Y.D. Han, Interior humidity of concrete under dry-wet cycles, J. Mater. Civil Eng. 24 (2012) 289-298.

[7] L.O. Nilsson, Interaction between microclimate and concrete - a prerequisite for deterioration, Constr. Build. Mater. 10 (1996) 301-308.

[8] Y. Zhang, M. Zhang, Transport properties in unsaturated cement-based materials – A review, Constr. Build. Mater. 72 (2014) 367–379.

[9] A.V. Saetta, R.V. Scotta, R.V. Vitaliani, Analysis of chloride diffusion into partially saturated concrete, ACI Mater. J. 90 (1993) 441-451.

[10] E.P. Nielsen, M.R. Geiker, Chloride diffusion in partially saturated cementitious material, Cem. Concr. Res. 33 (2003) 133-138.

[11] Y. Zhang, G. Ye, Chloride transport in partially saturated mortar made of blended cement, Proc. 14th Int. Congress on the Chemistry of Cement (ICCC2015), 13~16 October 2015, Beijing, China.

[12] N. Olsson, V. Baroghel-Bouny, L.O. Nilsson, M. Thiery, Non-saturated ion diffusion in concrete – A new approach to evaluate conductivity measurements, Cem. Concr. Compos. 40 (2013) 40-47.

[13] A. Buchwald, Determination of the ion diffusion coefficient in moisture and salt loaded masonry materials by impedance spectroscopy, 3rd Int. PhD symposium, Vienna, Austria, 2000.

[14] V. Baroghel-Bouny, M. Thiéry, X. Wang, Modelling of isothermal coupled moisture-ion transport in cementitious materials, Cem. Concr. Res. 41 (2011) 828-841.

739 [15] G.E. Archie, The electrical resistivity log as an aid in determining some reservoir
740 characteristics, Trans. AIME 146 (1942) 54-62.
741 [16] M. Zhang, G. Ye, K. van Breugel, Modeling of ionic diffusivity in non-saturated
742 cement-based materials using lattice Boltzmann method, Cem. Concr. Res. 42 (2012)
743 1524-1533.
744 [17] F. Rajabipour, In situ electrical sensing and material health monitoring of concrete
745 structures, PhD thesis, Purdue University, 2006.
746 [18] R.A. McKee, A generalization of the Nernst-Einstein equation for self-diffusion in high
747 defect concentration solids, Solid State Ionics 5 (1981) 133-136.
748 [19] L.P. Tang, L.O. Nilsson, P.A. Muhammed-Basheer, Resistance of Concrete to Chloride
749 Ingress: Testing and modelling, 2012, Padstow, Cornwall.
750 [20] E. Poulsen, L. Mejlbro, Diffusion of chloride in concrete: Theory and Application,
751 Taylor & Francis, 2006, London & New York.
752 [21] F.T. Manheim, L.S. Waterman, Initial Reports of the Deep Sea Drilling Project, 22
753 (1974) 663-670.
754 [22] R.C. Weast, Handbook of Chemistry and Physics, Cleveland, 1975.
755 [23] R.B. Polder, Test methods for onsite measurement of resistivity of concrete - a RILEM
756 TC-154 technical recommendation, Constr. Build. Mater. 15 (2000) 125-131.
757 [24] B.J. Christensen, Microstructure studies of hydrating Portland cement-based materials
758 using impedance spectroscopy, PhD thesis, Northwestern University, 1993.
759 [25] F. Rajabipour, Fundamental investigations on utilizing electrical sensing to improve
760 cycle modeling of concrete structure, MSc thesis, Purdue University, 2003.
761 [26] P.J. Tumidajski, A.S. Schumacher, S. Perron, P. Gu, J.J. Beaudoin, On the relationship
762 between porosity and electrical resistivity in cementitious systems, Cem. Concr. Res.
763 26 (1996) 539-544.

[27] S. Brunauer, The adsorption of gases and vapors, Physical Adsorption, Volume I, Princeton University Press, Princeton, 1943.

[28] Y. Zhang, M. Zhang, G. Ye, Influence of moisture condition on chloride diffusion in partially saturated ordinary Portland cement mortar, Mater. Struct. (2018) 51:36.

[29] A.V. Neimark, P.I. Ravikovitch, A. Vishnyakov, Bridging scales from molecular simulations to classical thermodynamics: density functional theory of capillary condensation in nano pores, J. Phys. Condens. Matter 15 (2003) 347-365.

[30] K.K. Aligizaki, Pore structure of cement-based materials: testing, interpretation and requirements, CRC Press, 2006.

[31] R.S. Barneyback Jr., S. Diamond, Expression and analysis of pore fluids from hardened cement pastes and mortars, Cem. Concr. Res. 11 (1981) 279-285.

[32] E.W. Washburn, Note on method of determining the distribution of pore size in porous materials, Proc. Natl. Acad. Sci. 7 (1921) 115-116.

[33] H.F.W. Taylor, A method for predicting alkali ion concentrations in cement pore solutions, Adv. Cem. Res. 1 (1987) 5-16.

[34] W. Chen, H.J.H. Brouwers, Alkali binding in hydrated Portland cement paste, Cem. Concr. Res. 40 (2010) 716-722.

[35] ASTM C642-13, Standard Test Method for Density, Absorption, and Voids in Hardened Concrete, February 2013.

[36] J.F. Young, W. Hansen, Volume relationship for C-S-H formation based on hydration stoichiometry, Mater. Res. Soc. Symp. Proc. 85 (1986) 313-322.

[37] Q. Zhang, G. Ye, Dehydration kinetics of Portland cement paste at high temperature, J. Therm. Anal. Calorim. 110 (2012) 153–158.

[38] B. Johannesson, Development of a generalized version of the Poisson–Nernst–Planck equations using the hybrid mixture theory: presentation of 2D numerical examples Transp. Porous Media, 85 (2010) 565-592.

[39] Y.K Yang, M.R. Wang, Pore-scale modeling of chloride ion diffusion in cement microstructures, Cem. Concr. Compos. 85 (2018) 92-104.

[40] Q.H. Nguyen, S. Lorente, A. Duhard-Barone, Effect of the pore size of cement based materials on ionic transport, Constr. Build. Mater. 147 (2017) 160-167.

[41] H. Mercado-Mendoza, S. Lorente, X. Bourbon, Ionic aqueous diffusion through unsaturated cementitious materials – A comparative study, Constr. Build. Mater. 51 (2014) 1-8.

[42] N. Olsson, B. Lothenbach, V. Baroghel-Bouny, L.O. Nilsson, Unsaturated ion diffusion in cementitious materials – The effect of slag and silica fume, Cem. Concr. Res. 108 (2018) 31-37.

[43] S. Mindess, J.F. Young, Concrete, Prentice-Hall, Englewood Cliffs, New York, 1981.

[44] G. Ye, Experimental study and numerical simulation of the development of the microstructure and permeability of cementitious materials, PhD thesis, Delft University of Technology, 2003.

[45] Y. Zhang, G. Ye, Experimental study of chloride diffusivity in unsaturated ordinary Portland cement mortar, 71st RILEM Week & ICACMS, INDIA, 3 - 8 September 2017.

[46] T. Ishida, K. Maekawa, T. Kishi, Enhanced modeling of moisture equilibrium and transport in cementitious materials under arbitrary temperature and relative humidity history, Cem. Concr. Res. 37 (2007) 565-578.

[47] J.M. de Burgh, S.J. Foster, Influence of temperature on water vapour sorption isotherms and kinetics of hardened cement paste and concrete, Cem. Concr. Res. 92 (2017) 37-55.

[48] Z.Q. Yu, Microstructure development and transport properties of Portland cement-fly ash binary systems-in view of service life predictions, PhD thesis, Delft University of Technology, 2015.